APL Photonics

Silicon nitride chirped spiral Bragg grating with large group delay

Cite as: APL Photonics **5**, 101302 (2020); https://doi.org/10.1063/5.0022963
Submitted: 26 July 2020 • Accepted: 29 September 2020 • Published Online: 09 October 2020

Zhenmin Du, Chao Xiang, Tingzhao Fu, et al.

Silicon nitride chirped spiral Bragg grating with large group delay

Cite as: APL Photon. 5, 101302 (2020); doi: 10.1063/5.0022963
Submitted: 26 July 2020 • Accepted: 29 September 2020 •
Published Online: 9 October 2020

Zhenmin Du,[1] Chao Xiang,[2] Tingzhao Fu,[1] Minghua Chen,[1] Sigang Yang,[1] John E. Bowers,[2,a)] and Hongwei Chen[1,a)]

AFFILIATIONS

[1]Beijing National Research Center for Information Science and Technology, Department of Electronic Engineering, Tsinghua University, Beijing 100084, China

[2]Department of Electrical and Computer Engineering, University of California Santa Barbara, Santa Barbara, California 93106, USA

[a)]**Authors to whom correspondence should be addressed:** bowers@ece.ucsb.edu and chenhw@tsinghua.edu.cn

ABSTRACT

As one of the most important optical filtering devices, Bragg gratings have been extensively used in various systems. A long Bragg grating is desired for many applications including frequency selection in semiconductor lasers and dispersion control for ultra-short pulses. As a prominent example, integrated spiral Bragg grating waveguides (SBGWs) have drawn much attention in the years. However, until now, the length of an integrated grating is still limited to a few milli-meters due to total waveguide loss. In this work, we propose and demonstrate a novel long chirped SBGW with waveguide loss as low as 0.05 dB/cm on a silicon nitride (Si_3N_4) platform. A 13.8 cm SBGW is fabricated, which is the longest on-chip waveguide grating reported so far. The SBGW's reflection bandwidth is 9.2 nm from 1556.3 nm to 1565.5 nm, and it provides a total of 1440 ps group delay, that is, −156.5 ps/nm of dispersion. The group delay response shows great linearity and temperature stability. This integrated device holds great potential for various applications including in-line dispersion compensation, optical true delay phase array, and microwave photonics.

A Bragg grating is one of the most important optical filtering devices, which could be used in many photonic applications, such as sensors,[1–3] communication,[4,5] dispersion control,[6,7] and photonic signal processing.[8,9] Recently, integrated waveguide Bragg gratings on silicon have attracted much attention.[10,11] Spiral Bragg grating waveguides (SBGWs) offer several advantages over straight Bragg gratings in fabrication uniformity and device footprint.[12] A long Bragg grating length is desired for many applications. For example, when integrated gratings are used as frequency selective mirrors for semiconductor lasers, long grating lengths are required to achieve ultra-narrow bandwidths and large extinction ratios (ERs).[13,14] Similarly, in order to control the dispersion of ultra-short pulse (~100 fs), the group delay slope and the bandwidth of the chirped Bragg grating must be large enough, which also requires the grating length to be as long as possible.[15] However, until now, the length of integrated gratings is still limited to few milli-meters, which is mainly due to the waveguide loss. In order to decrease losses, chirped SBGW for processing transverse magnetic (TM) modes in waveguides fabricated on a silicon-on-insulator (SOI) platform has been demonstrated.[12] Spectral responses of the TM modes are smoother and propagation losses are lower than TE modes in the same waveguides. However, considering that most of the current applications of integrated Bragg grating are based on TE modes, increasing the length of SBGW in the TM mode is not the fundamental solution. Therefore, the SBGW in our work is still designed for TE mode. In this work, a novel chirped SBGW fabricated on a silicon nitride platform is demonstrated. The waveguide dimension is specially designed so that the loss of the grating waveguide can be reduced to 0.05 dB/cm while the single TE mode transmission is maintained. The width and height of the Si_3N_4 waveguide are 2.8 μm and 0.09 μm, respectively. The SBGW structure is based on a spiral Si_3N_4 waveguide with periodic sidewall corrugation with a minimum radius of 800 μm. The length of the SBGW reaches 13.8 cm, which is the longest on-chip grating ever reported as far as we know. The filtering bandwidth is

about 9.2 nm from 1556.3 nm to 1565.5 nm, and a total of 1440 ps group delay is provided.

The total propagation loss of SBGW modes consists of several parts, including material absorption, Rayleigh scattering, interface scattering, substrate leakage, bending radiation, and crosstalk loss. Substrate leakage can be rendered negligible through the deposition of thick cladding layers. In addition, the crosstalk loss can be ignored when there is enough space between the waveguides. At the same time, the material absorption due to the N–H bond can be reduced below the detection limit of common measurement techniques by high temperature (1050 °C) annealing. Rayleigh scattering, accounting for a propagation loss on the order of 0.1 dB/km, is also negligible compared to interface scattering and bend radiation loss in waveguides. Thus, in order to reduce the loss of waveguide, it is necessary to reduce the interface scattering loss and select appropriate bending radius. By designing the geometry of the single-mode waveguide core layer, the loss can be reduced.[16–18]

A three-dimensional volume current method is used to calculate interfacial scattering loss.[19] For the simulation of waveguide bending loss, we transform the bent waveguide into an equivalent straight waveguide by the conformal mapping of the refractive index.[20,21] The loss of silicon nitride waveguide with thickness of 90 nm under different widths and bending radii is calculated and is shown in Fig. 1(b). With the increase in the bending radius, the loss of waveguide decreases dramatically and finally converges to a constant value. On the other hand, the larger the width of the waveguide is, the lower the overall loss. However, to ensure single-mode operation in 90 nm thick waveguides, the max waveguide width of 2.8 μm was used by design. When the bending radius of the waveguide is larger than 780 μm, the bending loss can be ignored and the loss of the waveguide can be regarded as the same as that of the straight waveguide, which is 4.87 dB/m. The measured waveguide loss is 5 dB/m.

Spiral Bragg gratings can wrap long Bragg gratings into compact areas, which will result in higher device yield. Figure 2(a) shows the schematic representation of the SBGW. The complete spiral consists of 40 semicircle silicon nitride waveguides. In order to avoid crosstalk between waveguides, the radius difference between two adjacent semicircle waveguides is set to 15 μm. The minimum radius r_0 of the semicircle silicon nitride waveguide is set to be 800 μm, and

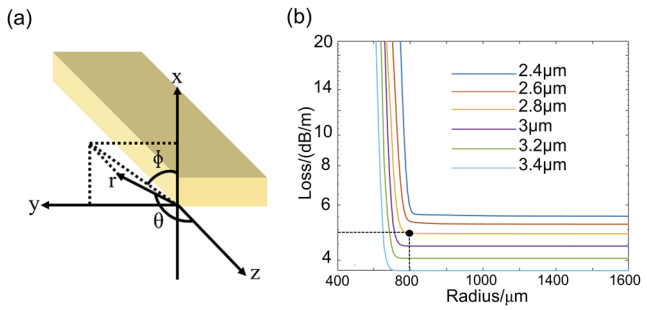

FIG. 1. (a) The coordinate system of the interface scattering loss model. (b) The loss of silicon nitride waveguide with a thickness of 90 nm under different widths and bending radii. The design of the SBGW is marked with a dot.

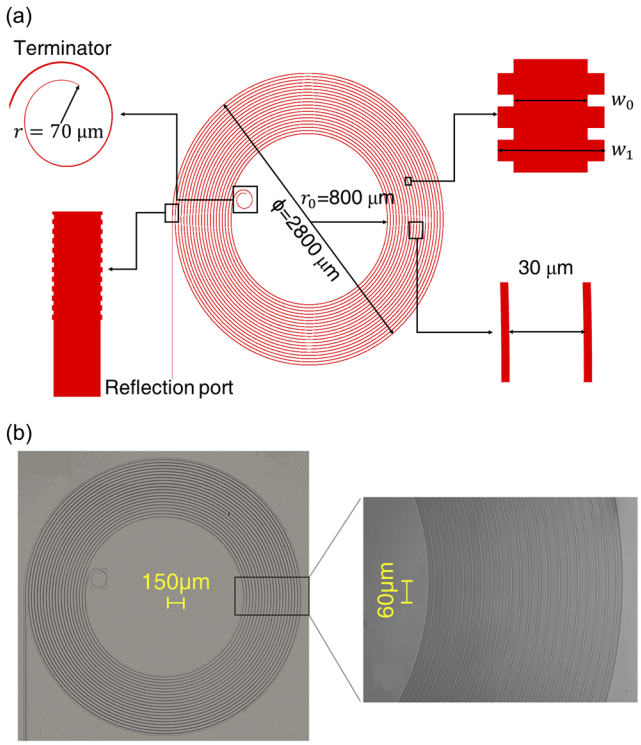

FIG. 2. (a) The diagram of SBGW. (b) Photomicrograph of chirped SBGW.

the overall size of the SBGW Φ is 2800 μm. In a SBGW, only the reflection port of the spiral is used, so a terminator is placed at the end of transmission port to dissipate light completely and reduce reflection. Once the waveguide trace is determined, the normal vector needs to be added onto the center path of the waveguide to get the refractive index perturbation as shown in Fig. 2. The normal vector refers to the structure with width w_1.[12] In our design, w_1 is 3 μm and w_0 is 2.8 μm.

The characteristics of the SBGW are determined by the length L, the chirp coefficient c, and the index perturbation Δn_{eff}. For a chirped Bragg grating, the period Λ will vary linearly along the length of the device, which makes the reflection wavelength also change according to the phase-match condition. However, for a SBGW, in addition to the period, the change in the effective refractive index caused by the change in the waveguide bending radius may also affect the reflection wavelength, which can be expressed as following:

$$\frac{d\lambda}{dz} = \frac{dn_{eff}}{dz} \times 2\Lambda + 2n_{eff} \times \frac{d\Lambda}{dz}, \quad (1)$$

where Λ is the period of the SBGW and n_{eff} is the effective refractive index of the waveguide. With the radius of the curved waveguides changing from 800 μm to 1400 μm, the $\frac{dn_{eff}}{dz}$ is 3×10^{-5}. The period of the SBGW starts with 531.5 nm and, then, reduces along the length to 528.1 nm. n_{eff} is 1.467 in SBGW. Therefore, the reflection wavelength is mainly determined by the second term in the right side of formula (1), which is the chirp (the periodic change per unit length).

Another important factor is the index perturbation of the chirped SBGW, defined as

$$\Delta n_{eff} = (n_1 - n_{eff})/2, \quad (2)$$

where n_1 is the effective refractive index of the normal vector. n_1 varies with w_1 as shown in Fig. 3(a). w_1 also causes additional loss due to the abrupt change in the refractive index.[22] It can be seen from Fig. 3(a) that the width of the normal vector has a great influence on the loss of SBGW. To fully understand the influence of parameters on the reflection spectrum of the chirped SBGW in detail, we introduced an accurate simulation approach using the transfer-matrix method (TMM).[23,24] Figures 4(a)–4(c) show the simulation results of SBGW using TMM when Δn_{eff} is 1×10^{-5}, 5×10^{-4}, and 1×10^{-3}, respectively. The grating length is set to be 13.8 cm, and the chirp coefficient c is set to be 2.46×10^{-8}. The waveguide loss is set to zero to show the effect of Δn_{eff} on the grating performance clearly. If Δn_{eff} is too large, there will be obvious ripples in the group delay curve, which will greatly affect the performance of the device. On the other hand, if Δn_{eff} is too small, the ripples of group delay curve will greatly reduce while the power of the reflection spectrum will decrease at the same time, i.e., insufficient grating reflection due to weak index pertubation.[25] Figure 3(b) shows the reflectivity and average group delay ripples (GDRs) of SBGW with different w_1. It can be seen that the high reflectivity and low GDRs are trade-offs. Therefore, considering the above factors, Δn_{eff} of our chirped SBGW is set to be 5×10^{-4}, and the corresponding w_1 is 3 μm. The GDRs are attributed to residual multiple reflections at the grating ends and can be significantly suppressed by a suitable apodization along its length.[26–29] To illustrate this intuitively, Fig. 4(d) shows the simulation result of an apodized SBGW. The apodization function is a hyperbolic tangent function and its expression is

$$\Delta n_{eff}(z) = \tanh\left(\frac{2Az}{L}\right) \times 5 \times 10^{-4} / \tanh(A), \quad (3)$$

where L = 13.8 cm is the length of SBGW and A = 3 is the modulation coefficient. The average GDR of apodized SBGW is only ±3.028 ps. The average GDR is defined as the average of the deviations between the group delay values at all wavelengths in the bandwidth and the ideal group delay curve. Figure 3(b) also shows the average GDR of the apodized grating at different w_1, which is greatly reduced.

Here, we use 248 nm deep-UV for optical lithography to create chirped SBGW structures. Compared to e-beam lithography (EBL), deep-UV lithography ensures the stability and uniformity for large-scale area processing.[30–33] The fabrication starts with a 100-mm diameter Si wafer with 8 μm thick thermal oxide. The oxide is grown in batches, and to maintain compatibility with a variety of waveguide thicknesses and waveguide confinements, the oxide is overly thick. The stoichiometric silicon nitride film of 90 nm thickness is grown by low pressure chemical vapor deposition (LPCVD). Although the

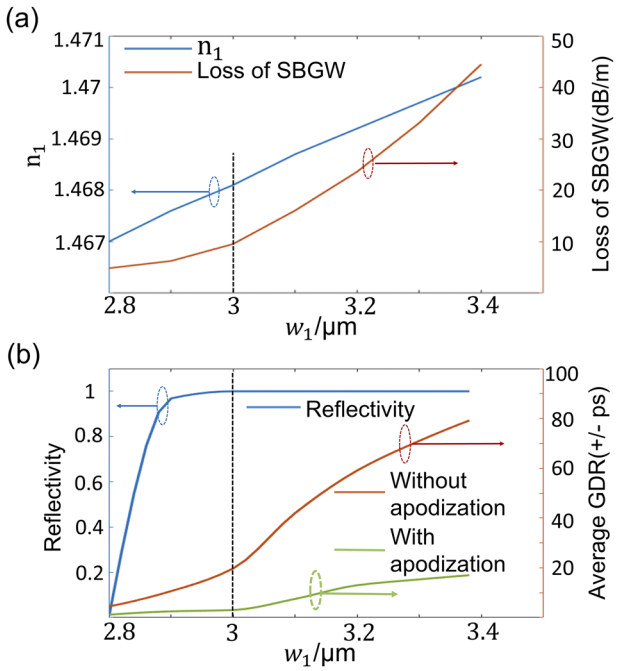

FIG. 3. (a) Values of n_1 and the loss of SBGW under different w_1. The dashed line represents the w_1 we used, which is 3 μm. (b) Change in reflectivity and average GDR of SBGW with and without apodization under different w_1.

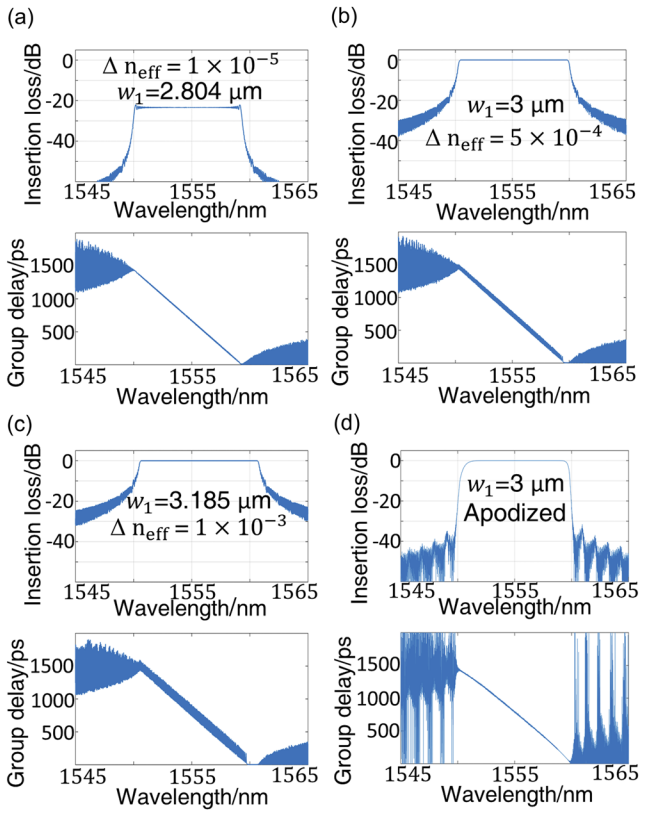

FIG. 4. (a) Simulated reflection spectrum and group delay of chirped SBGW at $\Delta n_{eff} = 1 \times 10^{-5}$. (b) Simulated reflection spectrum and group delay of chirped SBGW at $\Delta n_{eff} = 5 \times 10^{-4}$. (c) Simulated reflection spectrum and group delay of chirped SBGW at $\Delta n_{eff} = 1 \times 10^{-3}$. (d) Simulated reflection spectrum and group delay of apodized SBGW.

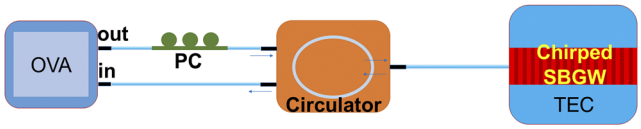

FIG. 5. Schematic illustration of the testing setup for the chirped SBGW.

internal stress of these layers is very high, the growth technology is deposited on both sides of the wafer to maintain the flatness of the wafer and achieve high-resolution lithography. Si_3N_4 SBGW is patterned followed by inductively coupled plasma (ICP) etching. The cladding consists of 2 μm silicon dioxide, which is deposited by plasma-enhanced chemical vapor deposition (PECVD) at 300 °C. The wafer is annealed at 1050 °C for 8 h and then diced for facet edge-coupled testing. Figure 2(b) shows the local microscopy picture of the chirped SBGW.

A Luna optical vector analyzer (OVA) and an optical circulator are used to test the chirped SBGW. The wavelength resolution of the OVA is 1.25 pm. Figure 5 shows the testing setup for chirped SBGW. The optical circulator is used to separate the incident light of the OVA from the light reflected by the chirped SBGW. Figure 6(a) shows the measured results of the chirped SBGW, and Fig. 6(b) shows the simulation results of the SBGW.

It can be seen that the spectral bandwidth of the chirped SBGW is 9.2 nm and the central wavelength is close to 1561 nm. The group delay measured by OVA is about 1440 ps. The measurement results of the actual chirped SBGW matches the simulation result very well in terms of bandwidth and total group delay, despite the reflection band wavelength of simulation and experiment is slightly different. This can be explained by the difference between experimental index data and designed value for upper SiO_2 cladding. The central wavelength of the reflection spectrum was designed to be 1555 nm. However, the experimental spectrum is red shifted by around 6 nm; this is mainly because in the actual processing, the index of the cladding layer upon the core layer will always be different from the expected value due to stress and other reasons. The refractive index of the actual cladding layer is about 1×10^{-2}, different from that in simulation. This difference leads to the shift of the reflection wavelength of the SBGW.

The shape of the reflection spectrum obtained from the experimental results is not horizontal, but inclined. The power difference between the minimum wavelength and the maximum wavelength in the bandwidth is nearly 2.7 dB, which is rare in previous studies. The grating length reaches 13.8 cm, which corresponds to 27.6 cm optical path difference across the entire band. As we mentioned above in Fig. 3(a), the estimated loss of the SBGW is about 9.54 dB/m. A 13.8 cm long SBGW will lead to a loss of about 2.63 dB, which results in an inclined reflection spectrum. From Fig. 6(a), it can be seen that the linearity of the group delay curve is good. The measured average GDR is only ±27 ps, which is close to the simulation result (±20 ps). The variation in GDR with wavelength obtained from experiment and simulations (with apodization and without apodization) is shown in Fig. 7. When we look into the zoom scale, experiment and simulation results show that there are

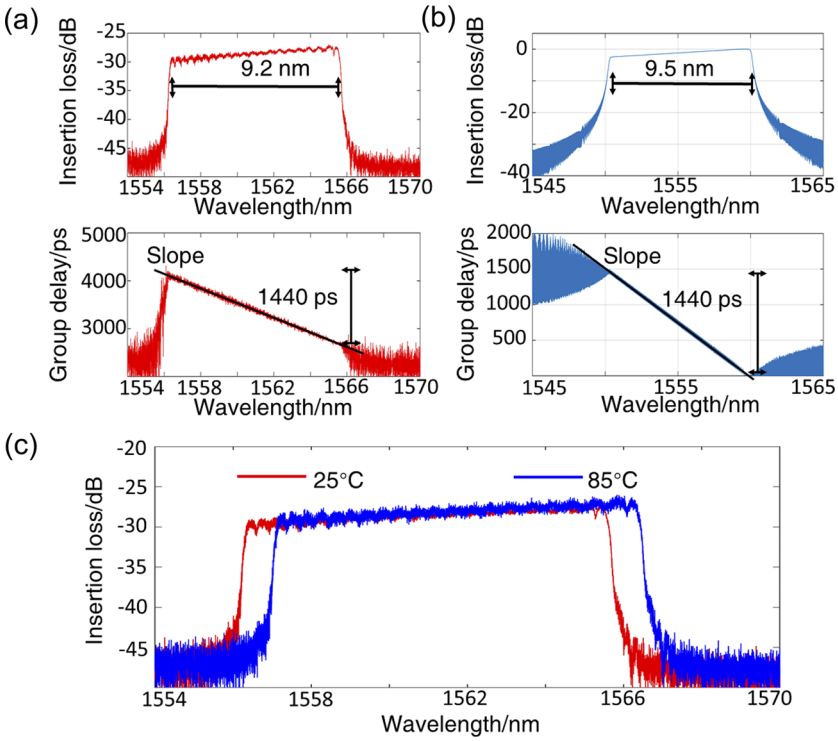

FIG. 6. (a) The measured reflection spectrum and group delay of the chirped SBGW. (b) The simulated reflection spectrum and group delay of the chirped SBGW. (c) The reflection spectrum of chirped SBGW at two different temperatures.

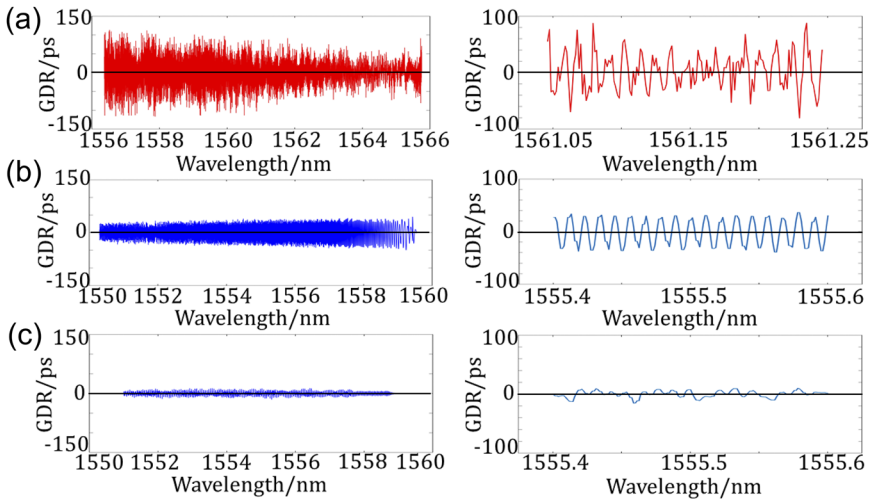

FIG. 7. (a) The variation of GDR with wavelength obtained in experiment and its magnified display in the range of 0.2 nm. (b) The variation of GDR with wavelength obtained in simulation without apodizaiton and its magnified display in the range of 0.2 nm. (c) The variation of GDR with wavelength obtained in simulation with apodizaiton and its magnified display in the range of 0.2 nm.

same 18 periods in the range of 0.2 nm, despite of the difference in amplitude.

The temperature stability of chirped SBGW is an important characteristic to evaluate its robustness.[34,35] In experiment, we changed the stage temperature of SBGW from 25 °C to 85 °C to observe the change of the reflection spectrum. Figure 6(c) shows the reflection spectrum of chirped SBGW at two different temperatures. The thermo-optic coefficient of silicon nitride material is about 2.5×10^{-5}/K. When the temperature changes from 25 °C to 85 °C, the refractive index of the silicon nitride material will increase from 1.987 to 1.9885, and the refractive index of silicon dioxide will increase from 1.444 to 1.4443. As a result, the n_{eff} of the waveguide is changed to 1.4686, while that of our preset grating is 1.4678 at 25 °C. In this case, the spectrum will shift 0.85 nm. We can see from Fig. 6(c) that the frequency spectrum measured in the experiment has shifted 0.8 nm with slight difference. This shows the high temperature stability of the chirped grating.

Table I shows a comparison of the chirped SBGWs reported in the recent years, on properties including the waveguide core material, grating length, bandwidth, and group delay. The temperature coefficients of wavelength are inferred from the data in the references. It can be seen that our SBGW has the longest length, largest group delay, and the best temperature stability.

In conclusion, a chirped SBGW on the silicon nitride platform with a length of 13.8 cm has been fabricated and characterized. It has waveguide loss as low as 0.05 dB/cm and achieves a 9.2 nm wide reflection bandwidth from 1556.3 nm to 1565.5 nm with a total of 1440 ps group delay and −156.5 ps/nm of dispersion. Under the appropriate chirp coefficient and index perturbation conditions, the chirped SBGW shows excellent performance. The group delay curve of the grating shows good linearity, and the temperature stability of the grating is excellent. This SBGW is promising in many fields, including microwave photonics, optical imaging, on-chip dispersion engineering, and management.

AUTHORS' CONTRIBUTIONS

Z.D. and C.X. contributed equally to this work.

ACKNOWLEDGMENTS

This work was supported by the National Key Research and Development Program of China under Contract No.

TABLE I. Comparison of chirped SBGWs.

Reference	Polarization	Core material	Length	Bandwidth (nm)	Total group delay (ps)	Temperature coefficient of reflection wavelength* (nm/°C)
36	TE	Silicon	3 mm	8.8	31.2	0.067
37	TE	Silicon	5 mm	15	50	0.067
12	TM	Silicon	4 mm	11.7	128.7	0.045
38	TE	Silicon	1 cm	1	250	0.023
This work	TE	Silicon nitride	13.8 cm	9.5	1440	0.013

2019YFB1803501, NSFC under Contract No. 61771284, and Beijing Natural Science Foundation under Contract No. L182043. The device is fabricated at the UCSB nanofabrication facility.

DATA AVAILABILITY

The data that support the findings of this study are available from the corresponding author upon reasonable request.

REFERENCES

[1]M. Fridrich, M. Fajkus, P. Mec, J. Nedoma, M. Kostelansky, and E. Bednar, Appl. Sci. **9**, 4796 (2019).
[2]X. Qiao, Z. Shao, W. Bao, and Q. Rong, Sensors **17**, 429 (2017).
[3]A. Pospori, C. A. F. Marques, D. Sáez-Rodríguez, K. Nielsen, O. Bang, and D. J. Webb, Opt. Fiber Technol. **36**, 68 (2017).
[4]S. Chettouh, A. El-Akrmi, H. Triki, and Y. Hamaizi, Optik **147**, 163 (2017).
[5]M. Tian, K. Nallapan, H. Guerboukha, and M. Skorobogatiy, Opt. Express **25**, 11009 (2017).
[6]D. B. Stegall and T. Erdogan, J. Opt. Soc. Am. **17**, 304 (2000).
[7]A. B. Dar and R. K. Jha, J. Mod. Opt. **64**, 555 (2017).
[8]Y. Liu, S. Fu, B. Malomed, I. Khoo, and J. Zhou, Appl. Sci. **7**, 556 (2017).
[9]C. Porzi, G. Serafino, P. Velha, P. Ghelfi, and A. Bogoni, J. Lightwave Technol. **35**, 4479 (2017).
[10]A. Li, J. Davis, and Y. Fainman, Opt. Lett. **45**, 644 (2020).
[11]D. J. Moss, V. G. Ta'eed, B. J. Eggleton, D. Freeman, S. Madden, M. Samoc, B. Luther-Davies, S. Janz, and D.-X. Xu, Appl. Phys. Lett. **85**, 4860 (2004).
[12]Z. Chen, J. Flueckiger, X. Wang, F. Zhang, H. Yun, Z. Lu, M. Caverley, Y. Wang, N. A. F. Jaeger, and L. Chrostowski, Opt. Express **23**, 25295 (2015).
[13]C. Xiang, P. A. Morton, and J. E. Bowers, Opt. Lett. **44**, 3825 (2019).
[14]C. Xiang, W. Jin, J. Guo, J. D. Peters, M. J. Kennedy, J. Selvidge, P. A. Morton, and J. E. Bowers, Optica **7**, 20 (2020).
[15]T. He, J. Demas, and S. Ramachandran, Opt. Lett. **42**, 2531 (2017).
[16]D. Xu, A. Delâge, J. H. Schmid, R. Ma, S. Wang, J. Lapointe, M. Vachon, P. Cheben, and S. Janz, Proc. SPIE. **8266**, 82660G (2012).
[17]J. F. Bauters, M. J. R. Heck, D. John, D. Dai, and J. E. Bowers, Opt. Express **19**, 3163 (2011).
[18]A. Frigg, A. Boes, G. Ren, I. Abdo, D.-Y. Choi, S. Gees, and A. Mitchell, Opt. Express **27**, 37795 (2019).
[19]T. Barwicz and H. A. Haus, J. Lightwave Technol. **23**, 2719 (2005).
[20]M. Heiblum and J. Harris, IEEE J. Quantum Electron. **11**, 75 (1975).
[21]P. Bienstman, E. Six, A. Roelens, M. Vanwolleghem, and R. Baets, IEEE Photonics Technol. Lett. **14**, 164 (2002).
[22]H.-M. Yang, S.-Y. Huang, C.-W. Lee, T.-S. Lay, and W.-H. Cheng, J. Lightwave Technol. **22**, 1395 (2004).
[23]B.-G. Kim and E. Garmire, J. Opt. Soc. Am. **9**, 132 (1992).
[24]G. W. Chern and L. A. Wang, J. Opt. Soc. Am. **16**, 2675 (1999).
[25]K. O. Hill and G. Meltz, J. Lightwave Technol. **15**, 1263 (1997).
[26]D. Pastor, J. Capmany, D. Ortega, V. Tatay, and J. Marti, J. Lightwave Technol. **14**, 2581 (1996).
[27]W. H. Loh, M. J. Cole, M. N. Zervas, S. Barcelos, and R. I. Laming, Opt. Lett. **20**, 2051 (1995).
[28]K. Ennser, N. Zervas, and R. L. Laming, IEEE J. Quantum Electron. **34**, 770 (1998).
[29]L. Poladian, Phys. Rev. E **48**, 4758 (1993).
[30]B. J. Lin, J. Vac. Sci. Technol. **12**, 1317 (1975).
[31]P. Dumon, W. Bogaerts, V. Wiaux, J. Wouters, S. Beckx, J. Van Campenhout, D. Taillaert, B. Luyssaert, P. Bienstman, and D. Van Thourhout, IEEE Photonics Technol. Lett. **16**, 1328 (2004).
[32]T. Iwayanagi, T. Kohashi, S. Nonogaki, T. Matsuzawa, K. Douta, and H. Yanazawa, IEEE Trans. Electron Devices **28**, 1306 (1981).
[33]Y. Kawamura, K. Toyoda, and S. Namba, J. Appl. Phys. **53**, 6489 (1982).
[34]F. N. Timofeev, G. Simin, M. S. Shatalov, S. A. Gurevich, P. Bayvel, R. Wyatt, I. Lealman, and R. Kashyap, Fiber Integr. Opt. **19**, 327 (2000).
[35]R. J. Espejo and S. D. Dyer, J. Lightwave Technol. **25**, 1777 (2007).
[36]M. Ma, Z. Chen, H. Yun, Y. Wang, X. Wang, N. A. F. Jaeger, and L. Chrostowski, IEEE Photonics Technol. Lett. **30**, 111 (2018).
[37]E. Mortazy, B. Le Drogoff, J. Azana, M. Chaker, and A. Tehranchi, in *International Workshop on Fibre and Optical Passive Components* (IEEE, 2011), pp. 1–4.
[38]I. Giuntoni, D. Stolarek, A. Gajda, J. Bruns, B. Tillack, K. Petermann, and L. Zimmermann, in *Advanced Photonics and Renewable Energy*, paper BMB4 (Optical Society of America, 2010).